

# Computational fluctuating fluid dynamics

John B. Bell

Center for Computational Sciences and Engineering  
Lawrence Berkeley National Laboratory  
Berkeley, California, 94720, USA

Alejandro L. Garcia  
Department of Physics  
San Jose State University  
San Jose, California, 95192, USA

Sarah A. Williams  
Carolina Center for Interdisciplinary Applied Mathematics  
Department of Mathematics  
University of North Carolina at Chapel Hill  
Chapel Hill NC 27599

September 11, 2008

**Abstract** This paper describes the extension of a recently developed numerical solver for the Landau-Lifshitz Navier-Stokes (LLNS) equations to binary mixtures in three dimensions. The LLNS equations incorporate thermal fluctuations into macroscopic hydrodynamics by using white-noise fluxes. These stochastic PDEs are more complicated in three dimensions due to the tensorial form of the correlations for the stochastic fluxes and in mixtures due to couplings of energy and concentration fluxes (e.g., Soret effect). We present various numerical tests of systems in and out of equilibrium, including time-dependent systems, and demonstrate good agreement with theoretical results and molecular simulation.

## 1 Introduction

Scientists are accustomed to viewing the world as deterministic and this mechanical point of view has been reinforced over and over by the technological successes of modern engineering. Yet this comfortable, predictable model cannot be applied directly to the microscopic world of nano-scale devices. This world is fluid, both in the hydrodynamic sense but also in the statistical sense. At the molecular scale, the state of a fluid is uncertain and constantly changing. At hydrodynamics scales the probabilistic effects are not quantum mechanical but entropic, that is, due to the spontaneous, random fluctuations.

Thermodynamic fluctuations are a textbook topic in equilibrium statistical mechanics [53] and have been studied extensively in non-equilibrium statistical mechanics [13] yet they are rarely treated in computational fluid dynamics. However, recently the fluid mechanics community has considered increasingly complex physical, chemical, and biological phenomena at the microscopic scale including systems for which significant interactions occur at scales ranging from molecular to macroscopic. Accurate modeling of such phenomena requires the correct representation of the spatial and temporal spectra of fluctuations, specifically when studying systems where the microscopic stochastics drive a macroscopic phenomenon. Some examples in which spontaneous fluctuations play an important role include the breakup of droplets in jets [16, 34, 48], Brownian molecular motors [2, 15, 46, 52], Rayleigh-Bernard convection (both single species [63] and mixtures [54]), Kolmogorov flow [5, 6, 42], Rayleigh-Taylor mixing [32, 33], combustion and explosive detonation [41, 51], and reaction fronts [47].

To incorporate thermal fluctuations into macroscopic hydrodynamics, Landau and Lifshitz introduced an extended form of the Navier-Stokes equations by adding stochastic flux terms [38]. The LLNS equations have been derived by a variety of approaches (see [8, 10, 20, 36, 38]) and have been extended to mixtures [12, 40, 49]. While they were originally developed for equilibrium fluctuations, specifically the Rayleigh and Brillouin spectral lines in light scattering, the validity of the LLNS equations for non-equilibrium systems has been derived [17] and verified in molecular simulations [26, 44, 45].

Several numerical approaches for the Landau-Lifshitz Navier-Stokes (LLNS) equations have been proposed. The earliest work is by Garcia, et al. [24] who developed a simple finite difference scheme for the linearized LLNS equations. By including the stochastic stress tensor of the LLNS equations into the lubrication equations Moseler and Landman [48] obtain good agreement with their molecular dynamics simulation in modeling the breakup of nanojets; recent extensions of this work confirm the important role of fluctuations and the utility of the stochastic hydrodynamic description [16, 34]. Coveney, De Fabritiis, Delgado-Buscalioni and co-workers have also used the LLNS equations in a hybrid scheme, coupling to a Molecular Dynamics calculation of a liquid. [14, 18, 19, 27].

Recently, we introduced a centered scheme for the LLNS equations based on interpolation schemes designed to preserve fluctuations combined with a third-order Runge-Kutta (RK3) temporal integrator. [4] Comparing with theory, we showed that the RK3 scheme correctly captures the spatial and temporal spectrum of equilibrium fluctuations. Further tests for non-equilibrium systems confirm that the RK3 scheme reproduces long-range correlations of fluctuations and stochastic drift of shock waves, as verified by comparison with molecular simulations. It is worth emphasizing that the ability of continuum methods to accurately capture fluctuations is fairly sensitive to the construction of the numerical scheme and our studies revealed that minor variations in the numerics can lead to significant changes in stability, accuracy, and overall behavior. We have also demonstrated that the RK3 scheme works well in a continuum-particle hybrid scheme in which the stochastic PDE solver is coupled to a Direct Simulation Monte Carlo (DSMC) particle code. [62]

The present paper extends our earlier work in several dimensions. First, we formulate the LLNS equations for a binary gas in a form suitable for the RK3 scheme. Second, the three dimensional construction of the scheme is explicitly outlined (earlier work was limited to one-dimensional systems). Finally, after we validate these extensions of the RK3 scheme in a variety of equilibrium and non-equilibrium scenarios, including the simulation of mixing in the Rayleigh-Taylor and Kelvin-Helmholtz instabilities.

## 2 Binary mixtures of ideal gases

This section summarizes the thermodynamic and hydrodynamic properties of binary mixtures of ideal gases, including the formulation of the stochastic Landau-Lifshitz Navier-Stokes (LLNS) equations for such mixtures. Though we focus on hard sphere ideal gases, primarily to allow direct comparison with molecular simulations, the methodology is easily extended to general fluids, as outlined at the end of this section.

### 2.1 Thermodynamic properties

Consider a gas composed of two molecular species, each being hard spheres but with differing molecular masses and diameters, specifically, with  $m_0$  and  $d_0$  for species zero and  $m_1$  and  $d_1$  for species one. For a volume  $V$  containing  $N_0$  and  $N_1$  particles of each species the mass density is  $\rho = \rho_0 + \rho_1$  with  $\rho_i = m_i N_i / V$ . We define the mass concentration,  $c$ , as  $\rho_0 = (1 - c)\rho$  and  $\rho_1 = c\rho$  (i.e.,  $c = 1$  is all species one). It will also be useful to work with the number concentration,  $c'$ , which is the mole fraction of red particles so  $c' = N_1 / (N_0 + N_1)$ . To convert between the two expressions for concentration we use

$$c = \frac{c'}{c' + m_R(1 - c')} = \frac{1}{(1 - m_R) + m_R/c'} \quad (1)$$

and

$$c' = \frac{m_R c}{1 - (1 - m_R)c} = \frac{m_R}{1/c - (1 - m_R)} \quad (2)$$

where  $m_R = m_0/m_1$  is the mass ratio.

The pressure is given by the law of partial pressures,  $P = P_0 + P_1$ , where  $P_i = N_i k_B T / V$  so

$$\begin{aligned} P &= \frac{(N_0 + N_1)k_B T}{V} = \left( \frac{\rho_0}{m_0} + \frac{\rho_1}{m_1} \right) k_B T \\ &= (\rho_0 R_0 + \rho_1 R_1) T = \rho((1-c)R_0 + cR_1) T \end{aligned} \quad (3)$$

where  $T$  is the temperature,  $R_i = k_B / m_i$ , and  $k_B$  is Boltzmann's constant. Since each species is a monatomic gas the heat capacity per particle is  $\frac{3}{2}k_B$  for constant volume and  $\frac{5}{2}k_B$  for constant pressure. The internal energy density is  $e = e_0 + e_1$  or,

$$\begin{aligned} e &= \frac{\frac{3}{2}(N_0 + N_1)k_B T}{V} = \frac{3}{2}(\rho_0 R_0 + \rho_1 R_1) T = \frac{P_0 + P_1}{\gamma - 1} = \frac{P}{\gamma - 1} \\ &= (C_{v,0}\rho_0 + C_{v,1}\rho_1) T = \rho(C_{v,0}(1-c) + C_{v,1}c) T \end{aligned} \quad (4)$$

where  $C_{v,i} = R_i / (\gamma - 1)$  is the heat capacity per unit mass and  $\gamma = 5/3$  is the ratio of the heat capacities. The total energy density is

$$E = e + \frac{1}{2} \frac{|\mathbf{J}|^2}{\rho} = \frac{P}{\gamma - 1} + \frac{1}{2} \rho |\mathbf{v}|^2 \quad (5)$$

where  $\mathbf{J}$  is the momentum density and the fluid velocity is  $\mathbf{v} = \mathbf{J} / \rho$ . Finally, the sound speed is  $c_s = \sqrt{\gamma P / \rho}$ .

One defines  $\mu$  as the difference in the chemical potential per unit mass for the two components (see [38], §58),

$$\mu = \frac{\mu_1}{m_1} - \frac{\mu_0}{m_0} \quad (6)$$

For a binary dilute gas the chemical potential may be written as [39]

$$\mu_i = k_B T \ln \frac{n_i}{n_0 + n_1} + k_B T \ln P + \chi_i(T) \quad (7)$$

For particles with no internal degrees of freedom

$$\chi_i(T) = -\frac{5}{2} k_B T \ln T - \mathcal{A} T \ln m_i \quad (8)$$

where  $\mathcal{A}$  is a complicated function of physical constants. Note that

$$\left( \frac{\partial \mu}{\partial c} \right)_{P,T} = \frac{k_B T}{c(1-c)(m_1(1-c) + m_0 c)} \quad (9)$$

for an ideal gas.

## 2.2 Hydrodynamic equations

To incorporate thermal fluctuations into macroscopic hydrodynamics Landau and Lifshitz introduced an extended form of the Navier-Stokes equations by adding stochastic flux terms [38]. The Landau-Lifshitz Navier-Stokes (LLNS) equations for a binary mixture may be written as [12, 40, 49]

$$\partial \mathbf{U} / \partial t + \nabla \cdot \mathbf{F} = \nabla \cdot \mathbf{D} + \nabla \cdot \mathbf{S} \quad (10)$$

where

$$\mathbf{U} = \begin{pmatrix} \rho \\ \rho_1 \\ \mathbf{J} \\ E \end{pmatrix} \quad (11)$$

is the vector of conserved quantities (density of total mass, species 1 mass, momentum and energy).

The hyperbolic and dissipative fluxes are given by

$$\mathbf{F} = \begin{pmatrix} \rho \mathbf{v} \\ \rho_1 \mathbf{v} \\ \rho \mathbf{v} \mathbf{v} + P \mathbf{I} \\ (E + P) \mathbf{v} \end{pmatrix} \quad \text{and} \quad \mathbf{D} = \begin{pmatrix} 0 \\ \mathbf{j} \\ \tau \\ Q + \mathbf{v} \cdot \tau + G \mathbf{j} \end{pmatrix} \quad (12)$$

The mass diffusion flux for species one is

$$\mathbf{j} = \rho D \left( \nabla c + \frac{k_T}{T} \nabla T + \frac{k_p}{P} \nabla P \right) \quad (13)$$

where  $D$ ,  $k_T$  and  $k_p$  are the mass diffusion, thermal diffusion, and baro-diffusion coefficients (see Appendix A). The stress tensor is  $\tau = \eta(\nabla \mathbf{v} + \nabla \mathbf{v}^T - \frac{2}{3} \mathbf{I} \nabla \cdot \mathbf{v})$  where  $\eta$  is the shear viscosity (the bulk viscosity is zero for an ideal gas); in component form we may write this as

$$\tau_{\alpha\beta} = \eta \left( \frac{\partial v_\beta}{\partial x_\alpha} + \frac{\partial v_\alpha}{\partial x_\beta} - \frac{2}{3} \delta_{\alpha\beta} \sum_\gamma^{x,y,z} \frac{\partial v_\gamma}{\partial x_\gamma} \right) \quad (14)$$

where  $\mathbf{v} = v_x \hat{\mathbf{x}} + v_y \hat{\mathbf{y}} + v_z \hat{\mathbf{z}}$ . Note that, except for the dependence of the viscosity coefficient on  $c$ , the momentum flux is unaffected by concentration. On the other hand, the energy flux is comprised of three contributions: the Fourier heat flux,  $Q = \kappa \nabla T$ , where  $\kappa$  is the thermal conductivity; the viscous heat dissipation,  $\mathbf{v} \cdot \tau$ , and a contribution that depends on the mass diffusion flux (see [38] §58 & 59),

$$G \mathbf{j} = \left[ k_T \left( \frac{\partial \mu}{\partial c} \right)_{P,T} - T \left( \frac{\partial \mu}{\partial T} \right)_{c,P} + \mu \right] \mathbf{j} \quad (15)$$

For an binary ideal gas mixture,

$$-T \left( \frac{\partial \mu}{\partial T} \right)_{c,P} + \mu = \frac{5}{2} k_B T \left( \frac{1}{m_1} - \frac{1}{m_0} \right) = \gamma (C_{v,1} - C_{v,0}) T = (C_{p,1} - C_{p,0}) T \quad (16)$$

so

$$G = k_T \left\{ \frac{k_B T}{c(1-c)(m_1(1-c) + m_0 c)} \right\} + (C_{p,1} - C_{p,0}) T \quad (17)$$

using eqn. (9).

To account for spontaneous fluctuations, the LLNS equations include a stochastic flux

$$\mathbf{S} = \begin{pmatrix} 0 \\ \mathcal{C} \\ \mathcal{S} \\ \mathcal{Q} + \mathbf{v} \cdot \mathcal{S} + G \mathcal{C} \end{pmatrix}, \quad (18)$$

where the stochastic concentration flux,  $\mathcal{C}$ , stress tensor  $\mathcal{S}$  and heat flux  $\mathcal{Q}$  have zero mean and covariances given by [12, 40]

$$\langle \mathcal{C}_i(\mathbf{r}, t) \mathcal{C}_j(\mathbf{r}', t') \rangle = \frac{2Dk_B \rho T}{\left( \frac{\partial \mu}{\partial c} \right)_{P,T}} \delta_{ij}^K \delta(\mathbf{r} - \mathbf{r}') \delta(t - t') \quad (19)$$

$$= 2D\rho [c(1-c)(m_1(1-c) + m_0 c)] \delta_{ij}^K \delta(\mathbf{r} - \mathbf{r}') \delta(t - t'),$$

$$\langle \mathcal{S}_{ij}(\mathbf{r}, t) \mathcal{S}_{kl}(\mathbf{r}', t') \rangle = 2k_B \eta T \left( \delta_{ik}^K \delta_{jl}^K + \delta_{il}^K \delta_{jk}^K - \frac{2}{3} \delta_{ij}^K \delta_{kl}^K \right) \delta(\mathbf{r} - \mathbf{r}') \delta(t - t'), \quad (20)$$

$$\langle \mathcal{Q}_i(\mathbf{r}, t) \mathcal{Q}_j(\mathbf{r}', t') \rangle = 2k_B \kappa T^2 \delta_{ij}^K \delta(\mathbf{r} - \mathbf{r}') \delta(t - t'), \quad (21)$$

and

$$\langle \mathcal{C}_k(\mathbf{r}, t) \mathcal{S}_{ij}(\mathbf{r}', t') \rangle = \langle \mathcal{C}_i(\mathbf{r}, t) \mathcal{Q}_j(\mathbf{r}', t') \rangle = \langle \mathcal{S}_{ij}(\mathbf{r}, t) \mathcal{Q}_k(\mathbf{r}', t') \rangle = 0 \quad (22)$$

Note that the covariance of the stress tensor is non-zero only when a pair of indices are equal and the other pair are equal as well. For example,

$$\langle \mathcal{S}_{xx} \mathcal{S}_{xx} \rangle = \frac{8}{3} k_B \eta T \delta(\mathbf{r} - \mathbf{r}') \delta(t - t'), \quad (23)$$

$$\langle \mathcal{S}_{xy} \mathcal{S}_{xy} \rangle = 2 k_B \eta T \delta(\mathbf{r} - \mathbf{r}') \delta(t - t'), \quad (24)$$

$$\langle \mathcal{S}_{xy} \mathcal{S}_{yx} \rangle = \langle \mathcal{S}_{xy} \mathcal{S}_{xy} \rangle, \quad (25)$$

$$\langle \mathcal{S}_{xx} \mathcal{S}_{yy} \rangle = -\frac{4}{3} k_B \eta T \delta(\mathbf{r} - \mathbf{r}') \delta(t - t'), \quad (26)$$

and  $\langle \mathcal{S}_{xx} \mathcal{S}_{xy} \rangle = \langle \mathcal{S}_{xx} \mathcal{S}_{yz} \rangle = \langle \mathcal{S}_{xy} \mathcal{S}_{xz} \rangle = 0$ .

### 2.3 Extension to General Fluids

The formulation above for dilute gases may easily be extended to the more general case by the following substitutions: First, the equation of state for the fluid replaces the ideal gas law in (3). Next, the energy density (4) is modified by according to the fluid's heat capacity (which may be a function of density and temperature). The chemical potential (7) and its derivatives are needed. Finally, the transport coefficients (see Appendix A) are required. Though the functional forms of these thermodynamic and hydrodynamic quantities will likely be more complicated, the LLNS equations (and the corresponding numerical scheme to solve them) are structurally unchanged.

## 3 Numerical Scheme

The third-order Runge-Kutta (RK3) scheme for the LLNS equations is presented in [4, 62] for single-species fluids in one-dimensional systems. This section presents the more general case of a binary mixture in three dimensions. The formulation in this more general case is complicated by the tensorial form of the stress tensor as well as having an additional equation for concentration (and a contribution from concentration in the energy equation).

The discretization in the RK3 scheme requires the interpolation of face-centered values from cell-centered values. As discussed in [4, 62], to compensate for the variance-reducing effect of the multi-stage Runge-Kutta algorithm we interpolate the conserved variables from their cell-centered values as,

$$\mathbf{U}_{i+1/2,j,k} = \alpha_1 (\mathbf{U}_{i,j,k} + \mathbf{U}_{i+1,j,k}) - \alpha_2 (\mathbf{U}_{i-1,j,k} + \mathbf{U}_{i+2,j,k}), \quad (27)$$

where

$$\alpha_1 = (\sqrt{7} + 1)/4 \quad \text{and} \quad \alpha_2 = (\sqrt{7} - 1)/4. \quad (28)$$

Hydrodynamic variables are always computed from conserved variables (e.g.,  $\mathbf{v} = \mathbf{J}/\rho$ ) for both cell and face-centered values.

The RK3 discretization can be written in the following three-stage form:

$$\begin{aligned} \mathbf{U}_{i,j,k}^{n+1/3} &= \mathbf{U}_{i,j,k}^n - \frac{\Delta t}{\Delta x} (\mathcal{F}_{i+\frac{1}{2},j,k}^n - \mathcal{F}_{i-\frac{1}{2},j,k}^n) \\ &\quad - \frac{\Delta t}{\Delta y} (\mathcal{G}_{i,j+\frac{1}{2},k}^n - \mathcal{G}_{i,j-\frac{1}{2},k}^n) - \frac{\Delta t}{\Delta z} (\mathcal{H}_{i,j,k+\frac{1}{2}}^n - \mathcal{H}_{i,j,k-\frac{1}{2}}^n) \\ \mathbf{U}_{i,j,k}^{n+2/3} &= \frac{3}{4} \mathbf{U}_{i,j,k}^n + \frac{1}{4} \mathbf{U}_j^{n+1/3} - \frac{1}{4} \left( \frac{\Delta t}{\Delta x} \right) (\mathcal{F}_{i+\frac{1}{2},j,k}^{n+1/3} - \mathcal{F}_{i-\frac{1}{2},j,k}^{n+1/3}) \\ &\quad - \frac{1}{4} \left( \frac{\Delta t}{\Delta y} \right) (\mathcal{G}_{i,j+\frac{1}{2},k}^{n+1/3} - \mathcal{G}_{i,j-\frac{1}{2},k}^{n+1/3}) - \frac{1}{4} \left( \frac{\Delta t}{\Delta z} \right) (\mathcal{H}_{i,j,k+\frac{1}{2}}^{n+1/3} - \mathcal{H}_{i,j,k-\frac{1}{2}}^{n+1/3}) \\ \mathbf{U}_{i,j,k}^{n+1} &= \frac{1}{3} \mathbf{U}_{i,j,k}^n + \frac{2}{3} \mathbf{U}_j^{n+2/3} - \frac{2}{3} \left( \frac{\Delta t}{\Delta x} \right) (\mathcal{F}_{i+\frac{1}{2},j,k}^{n+2/3} - \mathcal{F}_{i-\frac{1}{2},j,k}^{n+2/3}) \\ &\quad - \frac{2}{3} \left( \frac{\Delta t}{\Delta y} \right) (\mathcal{G}_{i,j+\frac{1}{2},k}^{n+2/3} - \mathcal{G}_{i,j-\frac{1}{2},k}^{n+2/3}) - \frac{2}{3} \left( \frac{\Delta t}{\Delta z} \right) (\mathcal{H}_{i,j,k+\frac{1}{2}}^{n+2/3} - \mathcal{H}_{i,j,k-\frac{1}{2}}^{n+2/3}), \end{aligned}$$

where

$$\begin{aligned}\mathcal{F}^m &= (\mathbf{F}(\mathbf{U}^m) - \mathbf{D}(\mathbf{U}^m) - \tilde{\mathbf{S}}(\mathbf{U}^m)) \cdot \hat{\mathbf{x}} \\ \mathcal{G}^m &= (\mathbf{F}(\mathbf{U}^m) - \mathbf{D}(\mathbf{U}^m) - \tilde{\mathbf{S}}(\mathbf{U}^m)) \cdot \hat{\mathbf{y}} \\ \mathcal{H}^m &= (\mathbf{F}(\mathbf{U}^m) - \mathbf{D}(\mathbf{U}^m) - \tilde{\mathbf{S}}(\mathbf{U}^m)) \cdot \hat{\mathbf{z}}\end{aligned}$$

The diffusive terms  $\mathbf{D}$  are discretized with standard second-order finite difference approximations; for example,

$$(\tau_{xx})_{i+\frac{1}{2},j,k} = \frac{4}{3}\eta_{i+\frac{1}{2},j,k} \frac{(v_x)_{i+1,j,k} - (v_x)_{i,j,k}}{\Delta x}$$

where  $\eta_{i+\frac{1}{2},j,k} = \eta(c_{i+\frac{1}{2},j,k}, T_{i+\frac{1}{2},j,k})$ .

As described in [4, 62], we take  $\tilde{\mathbf{S}} = \sqrt{2}\mathbf{S}$  to obtain the correct variance of the stochastic flux over the three stage averaging performed during a single time step in RK3; for example,

$$(\tilde{\mathbf{S}} \cdot \hat{\mathbf{x}})_{i+\frac{1}{2},j,k} = \sqrt{2} \begin{pmatrix} 0 \\ (\mathcal{C}_x)_{i+\frac{1}{2},j,k} \\ (\mathcal{S}_{xx})_{i+\frac{1}{2},j,k} + (\mathcal{S}_{yy})_{i+\frac{1}{2},j,k} + (\mathcal{S}_{zz})_{i+\frac{1}{2},j,k} \\ \left\{ (\mathcal{Q}_x)_{i+\frac{1}{2},j,k} + (v_x \mathcal{S}_{xx})_{i+\frac{1}{2},j,k} + (v_y \mathcal{S}_{yx})_{i+\frac{1}{2},j,k} \right. \\ \left. + (v_z \mathcal{S}_{zx})_{i+\frac{1}{2},j,k} + (G\mathcal{C}_x)_{i+\frac{1}{2},j,k} \right\} \end{pmatrix}$$

The stochastic flux terms are generated as

$$\begin{aligned}(\mathcal{C}_x)_{i+\frac{1}{2},j,k} &= \sqrt{\frac{1}{\Delta t V_c}} \sqrt{(D\rho A)_{i+1,j,k} + (D\rho A)_{i,j,k}} \mathfrak{R}_{i+\frac{1}{2},j,k} \\ (\mathcal{S}_{\alpha x})_{i+\frac{1}{2},j,k} &= \sqrt{\frac{k_B}{\Delta t V_c} \left(1 + \frac{1}{3}\delta_{\alpha x}^K\right)} \sqrt{(\eta T)_{i+1,j,k} + (\eta T)_{i,j,k}} \mathfrak{R}'_{i+\frac{1}{2},j,k} \\ (\mathcal{Q}_x)_{i+\frac{1}{2},j,k} &= \sqrt{\frac{k_B}{\Delta t V_c}} \sqrt{(\kappa T^2)_{i+1,j,k} + (\kappa T^2)_{i,j,k}} \mathfrak{R}''_{i+\frac{1}{2},j,k}\end{aligned}$$

where  $A = c(1-c)(m_1(1-c) + m_0c)$ ,  $V_c = \Delta x \Delta y \Delta z$  and the  $\mathfrak{R}$ 's are independent, Gaussian distributed random values with zero mean and unit variance. Note that  $\tilde{\mathbf{S}}$  is evaluated using the instantaneous values of the state variables, i.e., the noise here is multiplicative. As discussed in [4] the effect of this multiplicity was found to be negligible.

## 4 Numerical results

This section presents a series of computational examples, of progressively increasing sophistication, that demonstrate the accuracy and effectiveness of the stochastic RK3 algorithm. First we examine an equilibrium system, then several non-equilibrium examples, concluding with a demonstration of the effect of fluctuations on mixing in the Rayleigh-Taylor and Kelvin-Helmholtz instabilities.

### 4.1 Equilibrium system

First, we consider a uniform system at the reference density and temperature in a periodic domain; parameters for this equilibrium system are shown in Table 1. Four cases are investigated: two with a single species and two with a binary mixture ( $c = 1/2$ ,  $m_R = 3$ ,  $c' = 3/4$ ). For each of these cases the system is initialized with either zero net flow or an initial fluid velocity equal to the sound speed (i.e., Mach 1 flow). The molecular diameters and the molecular mass for species 1 in the binary mixture ( $m_1 = 6.63 \times 10^{-23}$ ) are chosen as to mimic Argon; the simulation parameters for the binary mixture are similar to those used in [4, 62] when  $c = 1$  and, in that case, yield STP conditions. In the single species case the molecular mass is  $m_* = \frac{3}{2}m_1$  so the average density and number of particles is the same in all four cases. The average number

Table 1: System parameters (in cgs units) for simulations of a dilute mixture gas at equilibrium in a periodic domain.

Molecular diameter (species 0 and 1)	$3.66 \times 10^{-8}$
Reference mass density	$1.78 \times 10^{-3}$
Reference temperature	273
Cell length ( $\Delta x = \Delta y = \Delta z$ )	$2.7 \times 10^{-6}$
Time step ( $\Delta t$ )	$1.0 \times 10^{-12}$

of particles per computational cell is  $\langle N \rangle = 351$  so the standard deviation of the fluctuations is about 5% of the mean value.

At thermodynamic equilibrium the variances and covariances of the mechanical variables are given by statistical mechanics [39] (see Appendix B for details),

$$\langle \delta \rho^2 \rangle = \zeta \frac{\langle \rho \rangle^2}{\langle N \rangle}; \quad \langle \delta \rho_1^2 \rangle = \frac{\langle c \rangle^2 \langle \rho \rangle^2}{\langle c' \rangle \langle N \rangle} \quad (29)$$

$$\langle \delta J^2 \rangle = \zeta \frac{\langle \rho \rangle^2}{\langle N \rangle} \langle u \rangle^2 + \frac{\langle \rho \rangle k_B \langle T \rangle}{V} \quad (30)$$

$$\langle \delta E^2 \rangle = \frac{\gamma}{(\gamma - 1)^2} \frac{\langle P \rangle^2}{\langle N \rangle} + \frac{\gamma}{\gamma - 1} \frac{\langle \rho \rangle k_B \langle T \rangle}{V} \langle u \rangle^2 + \frac{\zeta \langle \rho \rangle^2 \langle u \rangle^4}{4 \langle N \rangle} \quad (31)$$

$$\langle \delta \rho \delta J \rangle = \zeta \frac{\langle \rho \rangle^2}{\langle N \rangle} \langle u \rangle \quad (32)$$

$$\langle \delta \rho \delta E \rangle = \frac{1}{\gamma - 1} \frac{\langle \rho \rangle k_B \langle T \rangle}{V} + \frac{\zeta \langle \rho \rangle^2}{2 \langle N \rangle} \langle u \rangle^2 \quad (33)$$

$$\langle \delta J \delta E \rangle = \frac{\gamma}{\gamma - 1} \frac{\langle \rho \rangle k_B \langle T \rangle}{V} \langle u \rangle + \frac{\zeta \langle \rho \rangle^2}{2 \langle N \rangle} \langle u \rangle^3 \quad (34)$$

where

$$\zeta = 1 + \frac{(m_R - 1)^2}{m_R} \langle c \rangle (1 - \langle c \rangle) \quad (35)$$

Note that the variance of mass density in the binary mixture is greater by a factor of  $\zeta$  compared to a single species gas of particles with mass  $m_* = \langle \rho \rangle V / \langle N \rangle$ ; other variances and covariances are similarly enhanced. For the parameters we consider ( $c = 1/2, m_R = 3$ ) the value is  $\zeta = 4/3$ .

Tables 2 and 3 compare the results from one-dimensional and three-dimensional RK3 calculations, of 8000 cells and  $20 \times 20 \times 20$  cells respectively, with theoretical variances and covariances at equilibrium. These results, compiled from simulations running  $O(10^6)$  time steps, show that the RK3 scheme yields accurate results in all cases, with errors not exceeding four percent for the one-dimensional calculation. The errors in the binary mixture cases are comparable to those in for a single species with the largest discrepancies appearing in the energy variance in the 3D cases.

## 4.2 Non-equilibrium system: temperature gradient

A fluid under a non-equilibrium constraint, such as a velocity or temperature gradient, exhibits long-range correlations of fluctuations [13, 56]. In the case of a temperature gradient, the asymmetry of sound waves moving along versus against the gradient creates correlations among quantities, such as density and momentum fluctuations, that are independent at equilibrium. Molecular simulations also confirm the predicted correlations of non-equilibrium fluctuations for a fluid subjected to a temperature gradient [21, 44] and also to a velocity gradient [25]. Theoretical predictions of these correlations have also been confirmed by light scattering experiments yet the effects are subtle and difficult to measure accurately in the laboratory. It is precisely because the long-range correlation of non-equilibrium fluctuations is a subtle effect that we consider it a good test of the RK3 algorithm.

Binary Mixture (No Flow)	RK3	Theory	Percent Error
$\langle \delta \rho^2 \rangle$	1.1861e-008	1.20343e-008	-1.44%
$\langle \delta J^2 \rangle$	3.53767	3.4205	3.43%
$\langle \delta E^2 \rangle$	5.04799e+009	4.86102e+009	3.85%
$\langle \delta \rho_1^2 \rangle$	3.09915e-009	3.00858e-009	3.01%
$\langle \delta \rho \delta J \rangle$	1.15848e-007	0	0.06% (*)
$\langle \delta \rho \delta E \rangle$	5.06506	5.13074	-1.28%
$\langle \delta J \delta E \rangle$	101.695	0	0.08% (†)
Single Species (No Flow)	RK3	Theory	Percent Error
$\langle \delta \rho^2 \rangle$	8.92136e-009	9.02573e-009	-1.16%
$\langle \delta J^2 \rangle$	3.53984	3.4205	3.49%
$\langle \delta E^2 \rangle$	4.96694e+009	4.86102e+009	2.18%
$\langle \delta \rho_1^2 \rangle$	8.92136e-009	9.02573e-009	-1.16%
$\langle \delta \rho \delta J \rangle$	4.14024e-008	0	0.02% (*)
$\langle \delta \rho \delta E \rangle$	5.07371	5.13074	-1.11%
$\langle \delta J \delta E \rangle$	15.443	0	0.01% (†)
Binary Mixture (Mach 1 Flow)	RK3	Theory	Percent Error
$\langle \delta \rho^2 \rangle$	1.19657e-008	1.20343e-008	-0.57%
$\langle \delta J^2 \rangle$	11.0943	11.032	0.56%
$\langle \delta E^2 \rangle$	1.17017e+010	1.14736e+010	1.99%
$\langle \delta \rho_1^2 \rangle$	3.10713e-009	3.00858e-009	3.28%
$\langle \delta \rho \delta J \rangle$	0.000300865	0.000302663	-0.59%
$\langle \delta \rho \delta E \rangle$	8.87415	8.93673	-0.70%
$\langle \delta J \delta E \rangle$	311931	310784	0.37%
Single Species (Mach 1 Flow)	RK3	Theory	Percent Error
$\langle \delta \rho^2 \rangle$	8.97937e-009	9.02573e-009	-0.51%
$\langle \delta J^2 \rangle$	9.20775	9.12904	0.86%
$\langle \delta E^2 \rangle$	1.13227e+010	1.11726e+010	1.34%
$\langle \delta \rho_1^2 \rangle$	8.97937e-009	9.02573e-009	-0.51%
$\langle \delta \rho \delta J \rangle$	0.000225801	0.000226997	-0.53%
$\langle \delta \rho \delta E \rangle$	7.93204	7.98523	-0.67%
$\langle \delta J \delta E \rangle$	288230	286854	0.48%

Table 2: Variances and covariances at equilibrium as measured in the one-dimensional RK3 simulations and compared with eqns. (29)–(34). (\*) Percent error estimated as  $\langle \delta \rho \delta J \rangle / (\langle \delta \rho^2 \rangle \langle \delta J^2 \rangle)^{1/2}$ . (†) Percent error estimated as  $\langle \delta J \delta E \rangle / (\langle \delta J^2 \rangle \langle \delta E^2 \rangle)^{1/2}$

Binary Mixture (No Flow)	RK3	Theory	Percent Error
$\langle \delta \rho^2 \rangle$	1.15355e-008	1.20343e-008	-4.14%
$\langle \delta J^2 \rangle$	3.66285	3.42049	7.09%
$\langle \delta E^2 \rangle$	5.2962e+009	4.861e+009	8.95%
$\langle \delta \rho_1^2 \rangle$	3.23672e-009	3.00857e-009	7.58%
$\langle \delta \rho \delta J \rangle$	1.48917e-008	0	0.01% (*)
$\langle \delta \rho \delta E \rangle$	4.91364	5.13073	-4.23%
$\langle \delta J \delta E \rangle$	2.35081	0	0.00% (†)
Single Species (No Flow)	RK3	Theory	Percent Error
$\langle \delta \rho^2 \rangle$	8.65308e-009	9.0257e-009	-4.13%
$\langle \delta J^2 \rangle$	3.61695	3.42049	5.74%
$\langle \delta E^2 \rangle$	5.00158e+009	4.861e+009	2.89%
$\langle \delta \rho_1^2 \rangle$	8.65308e-009	9.0257e-009	-4.13%
$\langle \delta \rho \delta J \rangle$	1.2951e-008	0	0.01% (*)
$\langle \delta \rho \delta E \rangle$	4.91199	5.13073	-4.26%
$\langle \delta J \delta E \rangle$	4.31381	0	0.00% (†)
Binary Mixture (Mach 1 Flow)	RK3	Theory	Percent Error
$\langle \delta \rho^2 \rangle$	1.15684e-008	1.20343e-008	-3.87%
$\langle \delta J^2 \rangle$	10.9696	11.032	-0.57%
$\langle \delta E^2 \rangle$	1.18817e+010	1.14735e+010	3.56%
$\langle \delta \rho_1^2 \rangle$	3.23875e-009	3.00857e-009	7.65%
$\langle \delta \rho \delta J \rangle$	0.000290739	0.000302662	-3.94%
$\langle \delta \rho \delta E \rangle$	8.5808	8.9367	-3.98%
$\langle \delta J \delta E \rangle$	307710	310783	-0.99%
Single Species (Mach 1 Flow)	RK3	Theory	Percent Error
$\langle \delta \rho^2 \rangle$	8.67279e-009	9.0257e-009	-3.91%
$\langle \delta J^2 \rangle$	9.09505	9.12902	-0.37%
$\langle \delta E^2 \rangle$	1.12668e+010	1.11726e+010	0.84%
$\langle \delta \rho_1^2 \rangle$	8.67279e-009	9.0257e-009	-3.91%
$\langle \delta \rho \delta J \rangle$	0.000217972	0.000226996	-3.98%
$\langle \delta \rho \delta E \rangle$	7.66199	7.98521	-4.05%
$\langle \delta J \delta E \rangle$	283466	286853	-1.18%

Table 3: Variances and covariances at equilibrium as measured in the three-dimensional RK3 simulations and compared with eqns. (29)–(34). (\*) Percent error estimated as  $\langle \delta \rho \delta J \rangle / (\langle \delta \rho^2 \rangle \langle \delta J^2 \rangle)^{1/2}$ . (†) Percent error estimated as  $\langle \delta J \delta E \rangle / (\langle \delta J^2 \rangle \langle \delta E^2 \rangle)^{1/2}$

Non-equilibrium correlations have been analyzed for binary mixtures using the LLNS equations and approximations thereof (e.g., [13, 57]). However, to independently validate the RK3 algorithm we compare it with molecular simulations of a dilute gas. Specifically, we use the direct simulation Monte Carlo (DSMC) algorithm, a well-known method for computing gas dynamics at the molecular scale. [1, 7, 22] As in molecular dynamics, the state of the system in DSMC is given by the positions and velocities of particles. In each time step, the particles are first moved as if they did not interact with each other. After moving the particles and imposing any boundary conditions, collisions are evaluated by a stochastic process, conserving momentum and energy and selecting the post-collision angles from their kinetic theory distributions. For both equilibrium and non-equilibrium problems DSMC yields the physical spectra of spontaneous thermal fluctuations, as confirmed by excellent agreement with fluctuating hydrodynamic theory [24, 26, 44] and molecular dynamics simulations [43, 45].

The scenario we consider is a system with thermal walls at  $x = 0, L$  and periodic boundary conditions in the  $y$  and  $z$  directions. In the RK3 algorithm the boundary conditions for a rigid, impenetrable wall at constant temperature are implemented as follows: The wall is located at a cell edge, for example the wall at  $x = 0$  is at  $(i = \frac{1}{2}, j, k)$ . The grid is extended by two cells into the wall and the values at those cells are set at the beginning of each iteration. Specifically, the momentum is an odd function about the interface (because the wall is impenetrable) and the pressure is an even function (because it is rigid). The temperature of the boundary points is fixed by linear interpolation, for example,  $T_{0,j,k} = 2T_{1/2,j,k} - T_{1,j,k}$ . Because the concentration flux,  $\mathbf{j}$ , must be zero at the wall, given that the pressure is even, we have the condition

$$\nabla c = -\frac{k_T}{T} \nabla T \quad (36)$$

which is implemented by linear interpolation, for example,

$$c_{0,j,k} = c_{1,j,k} + \frac{k_T}{T_{1/2,j,k}} (T_{1,j,k} - T_{0,j,k}) \quad (37)$$

Note that if we neglect the Soret effect (i.e.,  $k_T = 0$ ) then the concentration is an even function at the interface. From  $c$ ,  $P$ , and  $T$  at the boundary condition cells, the mass and energy density are given by

$$\rho = \frac{P}{((1-c)R_0 + cR_1)T}, \quad E = \frac{P}{\gamma - 1} + \frac{1}{2} \frac{|\mathbf{J}|^2}{\rho} \quad (38)$$

where the fluid velocity is  $\mathbf{v} = \mathbf{J}/\rho$ . Note that if we neglect the Soret effect then  $\rho T$  is an even function.

Figure 1 shows that the mean temperature and concentration profiles obtained by RK3 are in good agreement with DSMC molecular simulations. There are significant Knudsen effects since the distance between the thermal walls is only about an order of magnitude larger than the equilibrium mean free path. As such, to obtain accurate results the wall temperatures in RK3 have to be adjusted to account for temperature jump. [59] As seen in Fig. 1, due to the Soret effect there is a significant concentration gradient induced by the temperature gradient.

The profiles of the variances of mass and energy density fluctuations,  $\langle \delta \rho_i^2 \rangle$  and  $\langle \delta E_i^2 \rangle$ , are shown in Fig. 2. The RK3 and DSMC data are in good agreement except near the walls where the variances in RK3 drop significantly. Finally, figure 3 shows the correlation of density-momentum correlations,  $\langle \delta \rho_i \delta J_{j^*} \rangle$  and momentum-energy correlations,  $\langle \delta J_i \delta E_{j^*} \rangle$ , where  $j^*$  is the center grid-point. Given that these long-range correlations are a subtle effect the data are in reasonable agreement. The major discrepancy is the under-prediction of the negative peak correlation near  $j^*$ .

### 4.3 Non-equilibrium system: mixing instabilities

Finally, we consider two classical instabilities that lead to mixing in a binary system. Specifically, we consider the Rayleigh-Taylor instability, which occurs when a heavy fluid rests upon a light fluid [58], and the Kelvin-Helmholtz instability that arises from the instability of a shear layer. The importance of fluctuations has recently been highlighted in the study of such instabilities by molecular simulations [32, 33].

Our simulations of the Rayleigh-Taylor instability are, as Lord Rayleigh described it in 1883 [55], for mixing in the presence of a constant gravitational field (Taylor later showed that the instability can also

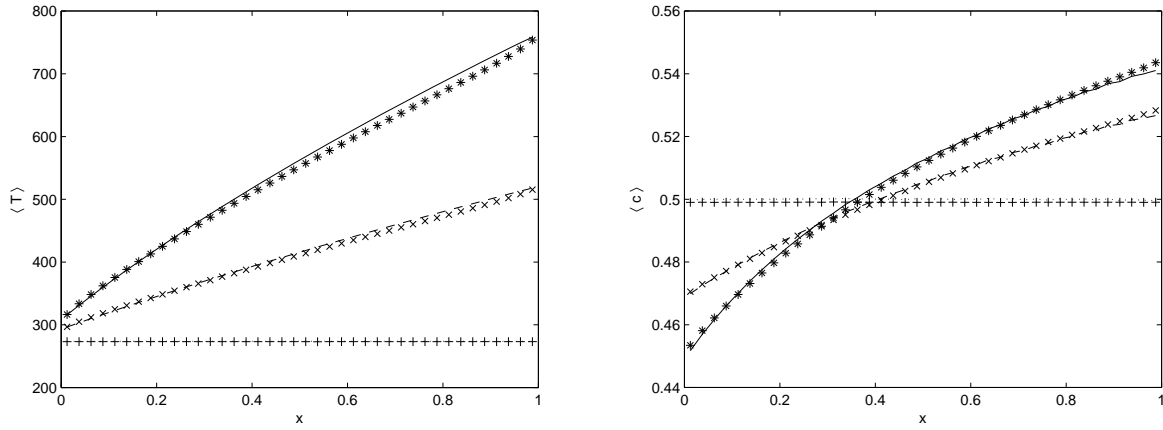


Figure 1: Mean temperature (left) and concentration (right) profiles from RK3 (lines) and DSMC (symbols) of a system with thermal walls. The three cases are: equilibrium (+ signs and dotted line); 2:1 temperature ratio (x-marks and dashed line); and 3:1 temperature ratio (\*-marks and solid line).

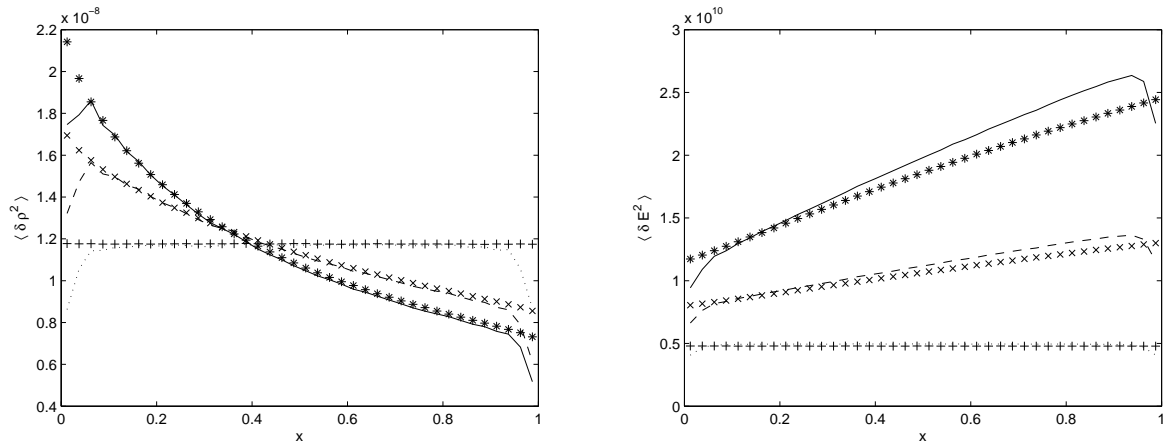


Figure 2: Variances of mass density fluctuations (left) and energy fluctuations (right) for a system subjected to a temperature gradient.

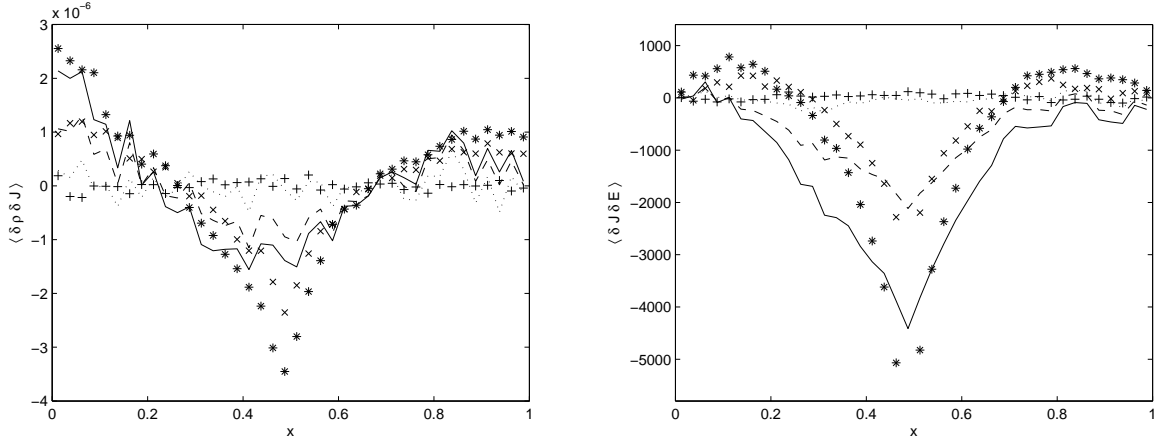


Figure 3: Spatial correlation of density- momentum fluctuations (left) and momentum-energy fluctuations (right) for a system subjected to a temperature gradient.

occur in accelerated fluids [60]). As in the earlier cases, the mass ratio is three with the heavier particles on top. The density and temperature are both increased to be approximately 10 times reference values and the pressure is initialized at hydrostatic equilibrium. We simulate a cubical domain  $12\mu\text{m}$  on a side discretized with a  $200 \times 200 \times 200$  grid. Gravitational acceleration is set to  $10^{12}\text{cm/sec}^2$  to enhance the formation of the instability at this microscopic scale. The boundary conditions on the top and bottom are planes of symmetry with periodic boundary conditions on the other four sides. The system is initialized with perfect symmetry and a flat interface, consequently, in the absence of the stochastic terms the Rayleigh-Taylor instability does not occur. Figure 4 shows the density and velocity fields after 8000 time steps, at which point some initial structure is first visible. Soon afterwards the structures become pronounced, as seen in Fig. 5.

As a second example, we consider the Kelvin-Helmholtz instability. The initial conditions are similar to those in the Rayleigh-Taylor case except that there is no gravitational acceleration and the particles of the two species have the same mass. The velocity is initialized to  $0.25c_s$  in the bottom half of the domain and to  $-0.25c_s$  in the top half of the domain. The domain is  $31.25\mu\text{m} \times 15.625\mu\text{m} \times 31.25\mu\text{m}$  and is discretized on a  $200 \times 100 \times 200$  grid. As in the Rayleigh-Taylor example, here, if there are no fluctuations, the instability will not form.

The development of the Kelvin-Helmholtz instability is shown in Figure 6. Initially, the viscous stress between the two streams slows the flow, inducing heating in the mixing region. As seen from the density and vertical velocity, this early mixing also generates sound waves that propagate normal to the interface. At this point only small perturbations are evident in velocity or concentration and there is little multidimensional structure. As the flow develops we begin to see the shear layer becoming unstable with evidence of vortical structures in all three fields. At the final time, a fully developed mixing layer is seen in all three fields as the shear layer continues to roll up.

## 5 Future Work

In this paper we have extended our basic LLNS method by including concentration as a hydrodynamic variable in order to model binary gas mixtures. A number of complicated terms must be introduced to accurately model unequal mass interactions, such as the Soret effect and baro-diffusion. The extension of the stochastic RK3 method to three-dimensions is also described. Finally, these extensions are validated in a variety of test cases and illustrated in two mixing instabilities triggered by fluctuations.

One avenue for future work is the incorporation of additional species and the introduction of chemical reactions. In a standard treatment of reactions at a continuum level, one assumes large populations of reacting species and a high-frequency of reaction. In this case, reactions can be modeled by continuum rate equations. For chemical systems these rates are typically of Arrhenius form with rates depending on

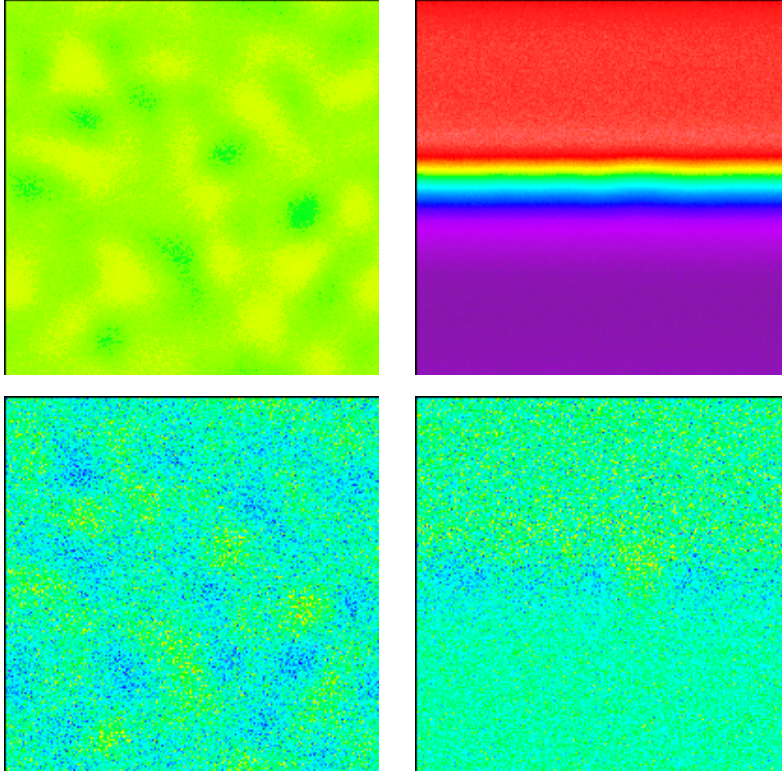


Figure 4: Mass density (top panels) and fluid velocity (lower panels) at 8000 steps for the Rayleigh Taylor instability induced by fluctuations from an initially flat surface. The left (right) panels are slices perpendicular (parallel) to the gravitational acceleration; the former is near the initial interface layer.

temperature and activation energies. At the mesoscopic scale some of these approximations break down due to the influence of spontaneous fluctuations. It should not be surprising that in reacting flows fluctuations have a more significant effect than in non-reacting systems due to the strong nonlinearities associated with the reaction pathways. This intuition is confirmed in a number of studies of these complex fluids [3, 35, 47, 50, 51].

Another avenue for exploration is the formulation of the Cahn-Hilliard system as an extension of the Landau-Lifshitz Navier-Stokes equations, taking the chemical potential as a sum of a thermodynamic term (the derivative of the Gibbs free energy), and a gradient energy term (attributed also to Van der Waals, and to Landau and Ginzburg). The Cahn-Hilliard equation describes the process of phase separation, such as when the two components of a binary fluid spontaneously separate. A number of studies have been published that solve the stochastic Cahn-Hilliard composition equations, decoupled from the continuity, momentum and energy equations (e.g., [9, 11, 29–31, 37, 61]). In these studies, the stochastic forcing is obtained from the fluctuation-dissipation theorem, however, it has not been determined that the resulting concentration fluctuations are consistent with statistical mechanics expectations (aside from structure factors and pair correlation functions – a subset of consistency requirements). The difficulty of achieving this correspondence for the simpler Landau-Lifshitz Navier-Stokes system strongly suggests that this correspondence is unlikely to be achieved in the Cahn-Hilliard system without special attention to the algorithmic construction. We are currently investigating such a construction with Prof. G. Miller of UC Davis.

Finally, the stability properties of the stochastic RK3 algorithm are not well understood, and the whole notion of stability is different than it is for deterministic schemes. For example, even at equilibrium, a rare fluctuation can cause a thermodynamic instability (e.g., a negative temperature which implies a complex sound speed), a mechanical instability (e.g., a negative mass density), or a purely numerical instability (e.g., division by zero). Capping the noises in the stochastic flux terms will not necessarily solve the problem

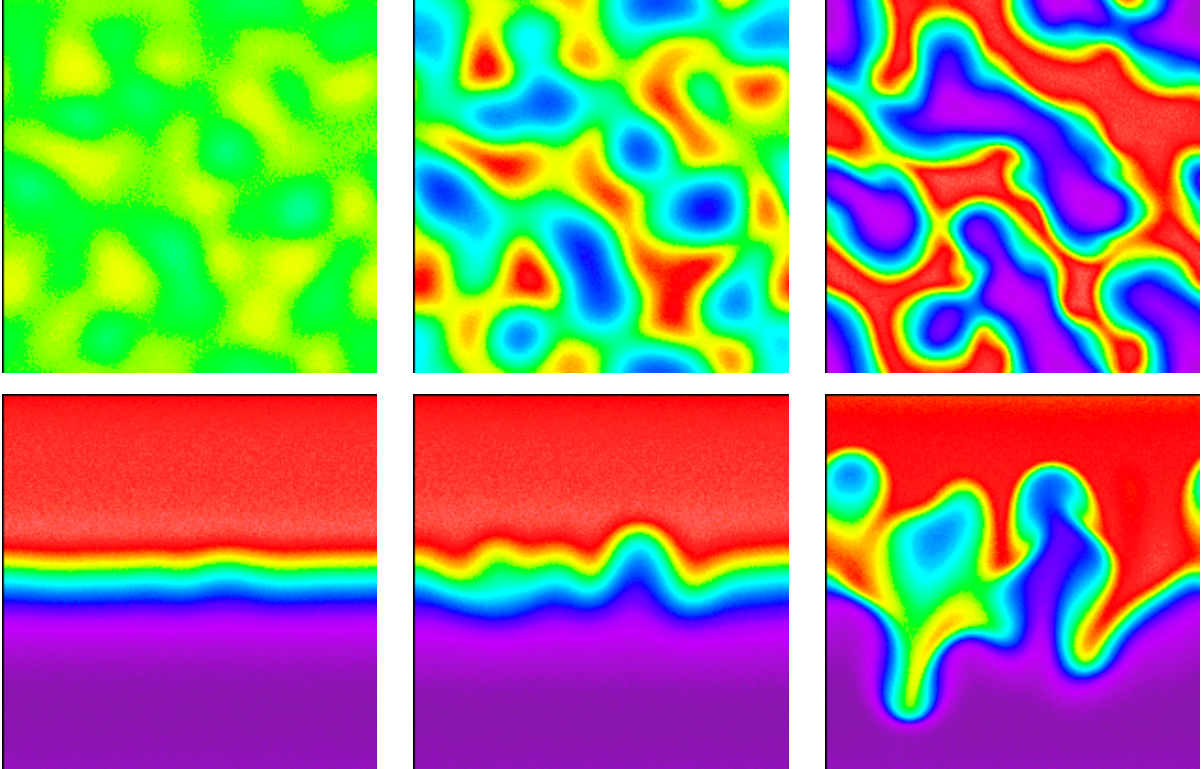


Figure 5: Mass density in the Rayleigh-Taylor instability at 10000, 14000, and 18000 steps (left to right). The top (bottom) panels are slices perpendicular (parallel) to the gravitational acceleration; the former is near the initial interface layer.

because the hydrodynamic variables are time-correlated so the numerical instability may not appear on a single step but rather as an accumulated effect. In addition, the efficiency of the method would be greatly improved if the scheme was able to use larger time steps. One particular type of approach we are pursuing is the development of implicit-explicit type discretizations that treat hyperbolic terms explicitly while treating diffusive terms implicitly. The key question for this type of discretization is how to treat stochastic terms in this framework to preserve the correct statistical properties of the solution. Addressing these issue will require the development of a better mathematical understanding of accuracy and stability properties for these type of systems.

## Appendix A: Transport Coefficients for a Binary Gas Mixture

The general expressions for the transport properties of a binary mixture of hard sphere gases are given in Hirshfelder, Curtis and Bird [28]; for completeness and the convenience of the reader they are reproduced in this appendix.

The viscosity is,

$$\eta = C_\eta \frac{1 + Z_\eta}{X_\eta + Y_\eta} \quad (39)$$

where

$$X_\eta = \frac{(1 - c')^2}{\eta_0} + \frac{2c'(1 - c')}{\eta_x} + \frac{c'^2}{\eta_1} \quad (40)$$

$$Y_\eta = \frac{3}{5} \left\{ \frac{(1 - c')^2}{\eta_0} \frac{m_0}{m_1} + \frac{2c'(1 - c')\eta_x}{\eta_0\eta_1} \frac{(m_0 + m_1)^2}{4m_0m_1} + \frac{c'^2}{\eta_1} \frac{m_1}{m_0} \right\} \quad (41)$$

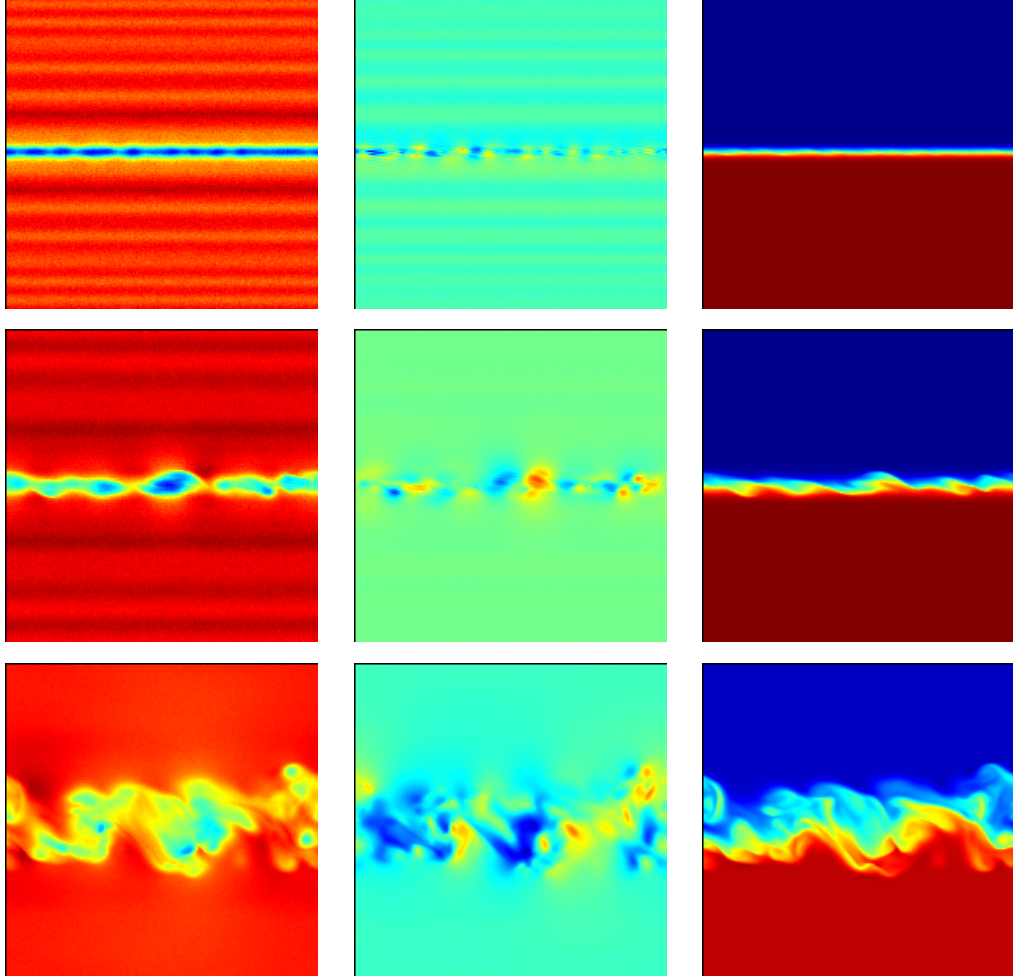


Figure 6: Slices normal to the transverse flow direction for the Kelvin-Helmholtz instability at 1000, 3000 and 8000 steps. The left panel is density, the center panel is vertical velocity and the right panel is concentration.

$$Z_\eta = \frac{3}{5} \left\{ (1 - c')^2 \frac{m_0}{m_1} + 2c'(1 - c') \left[ \frac{(m_0 + m_1)^2}{4m_0m_1} \left( \frac{\eta_x}{\eta_0} + \frac{\eta_x}{\eta_1} \right) - 1 \right] + c'^2 \frac{m_1}{m_0} \right\} \quad (42)$$

and with separate viscosity contributions of

$$\eta_i = \frac{5}{16d_i^2} \sqrt{\frac{m_i k_B T}{\pi}} \quad i = 0, 1, x \quad (43)$$

with the “cross” term values of  $m_x = 2m_0m_1/(m_0 + m_1)$  and  $d_x = (d_0 + d_1)/2$ . The Sonine polynomial correction factor is  $C_\eta = 1.016$  (see Table 8.3-2 in [28]).

The thermal conductivity is,<sup>1</sup>

$$\kappa = C_\kappa \frac{1 + Z_\kappa}{X_\kappa + Y_\kappa} \quad (44)$$

where  $C_\kappa = 1.025$  and

$$X_\kappa = \frac{(1 - c')^2}{\kappa_0} + \frac{2c'(1 - c')}{\kappa_x} + \frac{c'^2}{\kappa_1} \quad (45)$$

<sup>1</sup>Note that  $\lambda$  is used instead of  $\kappa$  in [28]

$$Y_\kappa = \frac{(1-c')^2 U_0}{\kappa_0} + \frac{2c'(1-c')U_Y}{\kappa_x} + \frac{c'^2 U_1}{\kappa_1} \quad (46)$$

$$Z_\kappa = (1-c')^2 U_0 + 2c'(1-c')U_Z + c'^2 U_1 \quad (47)$$

and

$$U_0 = \frac{4}{15} - \frac{17}{60} \frac{m_0}{m_1} + \frac{(m_0 - m_1)^2}{2m_0 m_1}; \quad U_1 = \frac{4}{15} - \frac{17}{60} \frac{m_1}{m_0} + \frac{(m_0 - m_1)^2}{2m_0 m_1}; \quad (48)$$

$$U_Y = \frac{4}{15} \frac{(m_0 + m_1)^2}{4m_0 m_1} \frac{\kappa_x^2}{\kappa_0 \kappa_1} - \frac{17}{60} + \frac{13}{32} \frac{(m_0 - m_1)^2}{m_0 m_1} \quad (49)$$

$$U_Z = \frac{4}{15} \left[ \frac{(m_0 + m_1)^2}{4m_0 m_1} \left( \frac{\kappa_x}{\kappa_0} + \frac{\kappa_x}{\kappa_1} \right) - 1 \right] - \frac{17}{60} \quad (50)$$

where

$$\kappa_i = \frac{15k_B}{4m_i} \eta_i \quad i = 0, 1, x \quad (51)$$

The coefficient of mass diffusion is

$$D = 6C_D \eta_x / 5\rho \quad (52)$$

where  $C_D = 1.133$ . The thermal diffusion coefficient,  $k_T$ , appears due to the Soret effect; it has the form,

$$k_T = C_S \frac{c'(1-c')}{6\kappa_x} \frac{S^{(1)}c' - S^{(0)}(1-c')}{X_\kappa + Y_\kappa} \quad (53)$$

where  $C_S = 1.299$  and

$$S^{(i)} = \frac{m_0 + m_1}{2m_{1-i}} \frac{\kappa_x}{\kappa_i} - \frac{15}{8} \frac{(-1)^i (m_1 - m_0)}{m_i} - 1 \quad (54)$$

Note that for particles of equal mass and diameter (i.e., when the particles are dynamically identical) then  $k_T = 0$ . This is evident from the argument that a temperature gradient will not separate distinguishable but physically identical particles (e.g., “red” and “blue” tagged particles); it’s also obtained from the equations above because  $S^{(0)} = S^{(1)} = 0$  in this case. Furthermore, if  $k_T > 0$  then species 1 moves towards the cold regions, which should occur when  $m_1 > m_0$ .

The baro-diffusion coefficient is given by

$$k_p = P \frac{(\partial\mu/\partial P)_{T,c}}{(\partial\mu/\partial c)_{P,T}} \quad (55)$$

For a binary dilute gas, we have,

$$k_p = (m_0 - m_1)c(1-c) \left( \frac{1-c}{m_0} + \frac{c}{m_1} \right) \quad (56)$$

Note that  $k_p$  is zero when  $m_0 = m_1$ .

## Appendix B: Variances in a Binary Gas Mixture

This appendix summarizes the variances and co-variances of the conserved variables,  $\rho$ ,  $\rho c$ ,  $\mathbf{J}$ , and  $E$ , at thermodynamic equilibrium. For hydrodynamic variables, such as  $\mathbf{v}$ ,  $T$ ,  $P$ , and  $c$ , the variances and covariances are obtained from these conserved (mechanical) variables, as described in [23].

The variance of the density of each species is the same as for a single, independent species, that is,  $\langle \delta\rho_i^2 \rangle = \rho_i^2 / N_i$ . The variance for the total density is thus

$$\langle \delta\rho^2 \rangle = \langle (\delta\rho_0 + \delta\rho_1)^2 \rangle = \langle \delta\rho_0^2 \rangle + \langle \delta\rho_1^2 \rangle = \frac{\langle \rho_0 \rangle^2}{\langle N_0 \rangle} + \frac{\langle \rho_1 \rangle^2}{\langle N_1 \rangle} = \zeta \frac{\langle \rho \rangle^2}{\langle N \rangle} \quad (57)$$

where

$$\zeta = \frac{(1 - \langle c \rangle)^2}{1 - \langle c' \rangle} + \frac{\langle c \rangle^2}{\langle c' \rangle} = 1 + \frac{(m_R - 1)^2}{m_R} \langle c \rangle (1 - \langle c \rangle) \quad (58)$$

gives the magnification of the density fluctuations due to the binary mixture. That is, the variance of mass density is greater by a factor of  $\zeta$  compared to a single species gas of particles with mass  $m = \langle \rho \rangle V / \langle N \rangle$ .

Since  $\rho_1$  is the same as  $\rho c$ ,

$$\langle \delta(\rho c)^2 \rangle = \langle \delta \rho_1^2 \rangle = \frac{\langle \rho_1 \rangle^2}{\langle N_1 \rangle} = \frac{\langle c \rangle^2 \langle \rho \rangle^2}{\langle c' \rangle \langle N \rangle} = \left( \langle c \rangle + \frac{1 - \langle c \rangle}{m_R} \right) \langle c \rangle \frac{\langle \rho \rangle^2}{\langle N \rangle} \quad (59)$$

We have a similar result for x-momentum density since  $\langle \delta J_i^2 \rangle = \langle J_i \rangle^2 / \langle N_i \rangle + \langle \rho_i \rangle^2 C_i^2 / \langle N_i \rangle$  where the thermal speed is  $C_i = \sqrt{k_B \langle T \rangle / m_i}$ . Thus,

$$\begin{aligned} \langle \delta J^2 \rangle &= \langle (\delta J_0 + \delta J_1)^2 \rangle = \langle \delta J_0^2 \rangle + \langle \delta J_1^2 \rangle \\ &= \zeta \frac{\langle J \rangle^2}{\langle N \rangle} + \frac{\langle \rho \rangle k_B \langle T \rangle}{V} = \zeta \frac{\langle \rho \rangle^2}{\langle N \rangle} \langle u \rangle^2 + \frac{\langle \rho \rangle k_B \langle T \rangle}{V} \end{aligned} \quad (60)$$

Note that the cross-terms are similar; for example  $\langle \delta \rho \delta J \rangle = \langle \delta \rho_0 \delta J_0 \rangle + \langle \delta \rho_1 \delta J_1 \rangle$ . Since  $\langle \delta \rho_i \delta J_i \rangle = \langle \rho_i \rangle \langle J_i \rangle / N_i$  then

$$\langle \delta \rho \delta J \rangle = \zeta \frac{\langle \rho \rangle \langle J \rangle}{\langle N \rangle} = \zeta \frac{\langle \rho \rangle^2}{\langle N \rangle} \langle u \rangle \quad (61)$$

When the mean fluid velocity is zero then the energy fluctuation is simply,

$$\delta E = \delta e_0 + \delta e_1 = \frac{\delta P_0 + \delta P_1}{\gamma - 1} \quad (62)$$

so

$$\langle \delta E^2 \rangle = \frac{\gamma}{(\gamma - 1)^2} \left( \frac{\langle P_0 \rangle^2}{\langle N_0 \rangle} + \frac{\langle P_1 \rangle^2}{\langle N_1 \rangle} \right) = \frac{\gamma}{(\gamma - 1)^2} \frac{\langle P \rangle^2}{\langle N \rangle} \quad (63)$$

since (see [39] §114)

$$\langle \delta P_i^2 \rangle = -k_B T \left( \frac{\partial P}{\partial V} \right)_S = \frac{k_B T \gamma P_i}{V} = \frac{\gamma P_i^2}{N_i} \quad (64)$$

and  $PV^\gamma = \text{const.}$  for an adiabatic process. The energy fluctuation expressions get somewhat messy if  $|\langle \mathbf{u} \rangle| \neq 0$  so we'll limit our attention to having the x-component,  $\langle J \rangle$ , be non-zero. We may now write  $\delta E = \delta E_0 + \delta E_1$  where

$$\delta E_i = \frac{\delta P_i}{\gamma - 1} + \frac{\langle J_i \rangle \cdot \delta J_i}{\langle \rho_i \rangle} - \frac{\delta \rho_i \langle J_i \rangle^2}{2 \langle \rho_i \rangle^2} \quad (65)$$

The variance is  $\langle \delta E^2 \rangle = \langle \delta E_0^2 \rangle + \langle \delta E_1^2 \rangle$  where

$$\langle \delta E_i^2 \rangle = \frac{\langle \delta P_i^2 \rangle}{(\gamma - 1)^2} + \frac{\langle J_i \rangle^2 \langle \delta J_i^2 \rangle}{\langle \rho_i \rangle^2} + \frac{\langle \delta \rho_i^2 \rangle \langle J_i \rangle^4}{4 \langle \rho_i \rangle^4} \quad (66)$$

$$\begin{aligned} &+ \frac{2 \langle \delta J_i \delta P_i \rangle \langle J_i \rangle}{(\gamma - 1) \langle \rho_i \rangle} - \frac{\langle \delta \rho_i \delta P_i \rangle \langle J_i \rangle^2}{(\gamma - 1) \langle \rho_i \rangle^2} - \frac{\langle \delta \rho_i \delta J_i \rangle \langle J_i \rangle^3}{\langle \rho_i \rangle^3} \\ &= \frac{1}{(\gamma - 1)^2} \langle \delta P_i^2 \rangle + \langle u \rangle^2 \langle \delta J_i^2 \rangle + \frac{1}{4} \langle u \rangle^4 \langle \delta \rho_i^2 \rangle \end{aligned} \quad (67)$$

$$+ \frac{2 R_i \langle T \rangle \langle u \rangle^2}{(\gamma - 1)} \langle \delta \rho_i^2 \rangle - \frac{R_i \langle T \rangle \langle u \rangle^2}{(\gamma - 1)} \langle \delta \rho_i^2 \rangle - \langle u \rangle^3 \langle \delta \rho_i \delta J_i \rangle \quad (68)$$

so

$$\begin{aligned} \langle \delta E^2 \rangle &= \frac{\gamma}{(\gamma - 1)^2} \frac{\langle P \rangle^2}{\langle N \rangle} + \langle u \rangle^2 \left[ \zeta \frac{\langle J \rangle^2}{\langle N \rangle} + \frac{\langle \rho \rangle k_B \langle T \rangle}{V} \right] + \frac{1}{4} \langle u \rangle^4 \left[ \zeta \frac{\langle \rho \rangle^2}{\langle N \rangle} \right] \\ &+ \langle u \rangle^2 \frac{\langle \rho \rangle k_B \langle T \rangle}{(\gamma - 1) V} - \langle u \rangle^3 \left[ \zeta \frac{\langle \rho \rangle \langle J \rangle}{\langle N \rangle} \right] \end{aligned} \quad (69)$$

$$= \frac{\gamma}{(\gamma - 1)^2} \frac{\langle P \rangle^2}{\langle N \rangle} + \frac{\gamma}{\gamma - 1} \frac{\langle \rho \rangle k_B \langle T \rangle}{V} \langle u \rangle^2 + \frac{\zeta}{4} \frac{\langle \rho \rangle^2 \langle u \rangle^4}{\langle N \rangle} \quad (70)$$

Finally, the covariances of the remaining variables are

$$\langle \delta\rho\delta E \rangle = \frac{1}{\gamma-1} \frac{\langle \rho \rangle k_B \langle T \rangle}{V} + \frac{\zeta \langle \rho \rangle^2}{2 \langle N \rangle} \langle u \rangle^2 \quad (71)$$

and

$$\langle \delta J \delta E \rangle = \frac{\gamma}{\gamma-1} \frac{\langle \rho \rangle k_B \langle T \rangle}{V} \langle u \rangle + \frac{\zeta \langle \rho \rangle^2}{2 \langle N \rangle} \langle u \rangle^3 \quad (72)$$

It is easy to verify that if  $m_0 = m_1$  then all the expressions above are the same as for a single species since in that case  $c = c'$  and  $\zeta(c, m_R) = 1$ .

## References

- [1] F.J. Alexander and A.L. Garcia. The direct simulation monte carlo method. *Computers in Physics*, 11(6):588–593, 1997.
- [2] R. D. Astumian and P. Hanggi. Brownian motors. *Physics Today*, pages 33–39, November 2002.
- [3] F. Baras, G. Nicolis, M. Malek Mansour, and J. W. Turner. Stochastic theory of adiabatic explosion. *Journal of Statistical Physics*, 32(1):1–23, 1983.
- [4] J.B. Bell, A.L. Garcia, and S.A. Williams. Numerical methods for the stochastic Landau-Lifshitz Navier-Stokes equations. *Phys. Rev. E*, 76:016708, 2007.
- [5] I. Bena, F. Baras, and M. Malek Mansour. Hydrodynamic fluctuations in the Kolmogorov flow: Non-linear regime. *Phys. Rev. E*, 62(5):6560–6570, Nov 2000.
- [6] I. Bena, M. Malek Mansour, and F. Baras. Hydrodynamic fluctuations in the Kolmogorov flow: Linear regime. *Phys. Rev. E*, 59(5):5503–5510, May 1999.
- [7] G.A. Bird. *Molecular Gas Dynamics and the Direct Simulation of Gas Flows*. Clarendon, Oxford, 1994.
- [8] M. Bixon and R. Zwanzig. Boltzmann-Langevin equation and hydrodynamic fluctuations. *Phys. Rev.*, 187(1):267–272, Nov 1969.
- [9] D. Blömker, S. Maier-Paape, and T. Wanner. Second phase spinodal decomposition for the Cahn-Hilliard-Cook equation. *T. Am. Math. Soc.*, 360:449–489, 2008.
- [10] E. Calzetta. Relativistic fluctuating hydrodynamics. *Class. Quantum Grav.*, 15:653, 1998.
- [11] H.D. Ceniceros and G.O. Mohler. A practical splitting method for stiff SDEs with application to problems with small noise. *Multiscale Model. Simul.*, 6:212–227, 2007.
- [12] C. Cohen, J.W.H. Sutherland, and J.M. Deutch. Hydrodynamic correlation functions for binary mixtures. *Phys. Chem. Liquids*, 2:213–235, 1971.
- [13] J. M. Ortiz de Zarate and J. V. Sengers. *Hydrodynamic Fluctuations in Fluids and Fluid Mixtures*. Elsevier Science, 2007.
- [14] R. Delgado-Buscalioni and G. De Fabritiis. Embedding molecular dynamics within fluctuating hydrodynamics in multiscale simulations of liquids. *Physical Review E (Statistical, Nonlinear, and Soft Matter Physics)*, 76(3):036709, 2007.
- [15] C. Van den Broeck, R. Kawai, and P. Meurs. Exorcising a Maxwell demon. *Phys. Rev. Lett.*, 93:090601, 2004.
- [16] J. Eggers. Dynamics of liquid nanojets. *Physical Review Letters*, 89(8):084502, 2002.
- [17] P. Español. Stochastic differential equations for non-linear hydrodynamics. *Physica A*, 248:77, 1998.

- [18] G. De Fabritiis, R. Delgado-Buscalioni, and P. V. Coveney. Multiscale modeling of liquids with molecular specificity. *Physical Review Letters*, 97(13):134501, 2006.
- [19] G. De Fabritiis, M. Serrano, R. Delgado-Buscalioni, and P. V. Coveney. Fluctuating hydrodynamic modeling of fluids at the nanoscale. *Physical Review E (Statistical, Nonlinear, and Soft Matter Physics)*, 75(2):026307, 2007.
- [20] R. F. Fox and G. E. Uhlenbeck. Contributions to non-equilibrium thermodynamics. I. Theory of hydrodynamical fluctuations. *Phys. Fluids*, 13(8):1893–1902, 1970.
- [21] A.L. Garcia. Nonequilibrium fluctuations studied by a rarefied gas simulation. *Phys. Rev. A*, 34:1454, 1986.
- [22] A.L. Garcia. *Numerical Methods for Physics*. Prentice Hall, 2nd edition, 2000.
- [23] A.L. Garcia. Estimating hydrodynamic quantities in the presence of microscopic fluctuations. *Communications in Applied Mathematics and Computational Science*, page (to appear), 2006.
- [24] A.L. Garcia, M. Malek Mansour, G. Lie, and E. Clementi. Numerical integration of the fluctuating hydrodynamic equations. *Journal of Statistical Physics*, 47:209, 1987.
- [25] A.L. Garcia, M.M. Mansour, G.C. Lie, M. Mareschal, and E. Clementi. Hydrodynamic fluctuations in a dilute gas under shear. *Physical Review A*, 36:4348–4355, 1987.
- [26] A.L. Garcia and C. Penland. Fluctuating hydrodynamics and principal oscillation pattern analysis. *J. Stat. Phys.*, 64:1121, 1991.
- [27] G. Giupponi, G. De Fabritiis, and Peter V. Coveney. Hybrid method coupling fluctuating hydrodynamics and molecular dynamics for the simulation of macromolecules. *The Journal of Chemical Physics*, 126(15):154903, 2007.
- [28] J.O. Hirschfelder, C.F. Curtis, and R.B. Bird. *Molecular Theory of Gases and Liquids*. John Wiley & Sons, 1954.
- [29] D.J. Horntrop. Mesoscopic simulation of Ostwald ripening. *J. Comp. Phys.*, 218:429–441, 2006.
- [30] D.J. Horntrop. Spectral method study of domain coarsening. *Phys. Rev. E*, 75:046703–1–8, 2007.
- [31] M. Ibañes, J García-Ojalvo, R. Toral, and J.M. Sancho. Dynamics and scaling of noise-induced domain growth. *Eur. Phys. J. B*, 18:663–673, 2000.
- [32] K. Kadau, T.C. Germann, N.G. Hadjiconstantinou, P.S. Lomdahl, G. Dimonte, B.L. Holian, and B.J. Alder. Nanohydrodynamics simulations: An atomistic view of the Rayleigh-Taylor instability. *PNAS*, 101(16):5851–5855, 2004.
- [33] K. Kadau, C. Rosenblatt, J.L. Barber, T.C. Germann, Z. Huang, P. Carls, and B.J. Alder. The importance of fluctuations in fluid mixing. *PNAS*, (To Appear), 2007.
- [34] W. Kang and U. Landman. Universality crossover of the pinch-off shape profiles of collapsing liquid nanobridges in vacuum and gaseous environments. *Physical Review Letters*, 98(6):064504, 2007.
- [35] A.L. Kawczynski and B. Nowakowski. Stochastic transitions through unstable limit cycles in a model of bistable thermochemical system. *Phys. Chem. Chem. Phys.*, 10:289 – 296, 2008.
- [36] G.E. Kelly and M.B. Lewis. Hydrodynamic fluctuations. *Physics of Fluids*, 14(9):1925–1931, 1971.
- [37] A. M. Lacasta, J. M. Sancho, and F. Sagués. Phase separation dynamics under stirring. *Phys. Rev. Lett.*, 75:1791–1974, 1995.
- [38] L.D. Landau and E.M. Lifshitz. *Fluid Mechanics*, volume 6 of *Course of Theoretical Physics*. Pergamon, 1959.

- [39] L.D. Landau and E.M. Lifshitz. *Statistical Physics*, volume 5 of *Course of Theoretical Physics*. Pergamon, third ed., part 1 edition, 1980.
- [40] B.M. Law and J.C. Nieuwoudt. Noncritical liquid mixtures far from equilibrium: The Rayleigh line. *Phys. Rev. A*, 40(7):3880–3885, 1989.
- [41] A. Lemarchand and B. Nowakowski. Fluctuation-induced and nonequilibrium-induced bifurcations in a thermochemical system. *Molecular Simulation*, 30(11-12):773–780, 2004.
- [42] M. Malek Mansour, C. Van den Broeck, I. Bena, and F. Baras. Spurious diffusion in particle simulations of the Kolmogorov flow. *EPL (Europhysics Letters)*, 47(1):8–13, 1999.
- [43] M. Malek Mansour, A.L. Garcia, J.W. Turner, and M. Mareschal. On the scattering function of simple fluids in finite systems. *J. Stat. Phys.*, 52:295, 1988.
- [44] M.M. Mansour, A.L. Garcia, G.C. Lie, and E. Clementi. Fluctuating hydrodynamics in a dilute gas. *Physical Review Letters*, 58:874–877, 1987.
- [45] M. Mareschal, M.M. Mansour, G. Sonnino, and E. Kestemont. Dynamic structure factor in a nonequilibrium fluid: A molecular-dynamics approach. *Physical Review A*, 45:7180–7183, May 1992.
- [46] P. Meurs, C. Van den Broeck, and A.L. Garcia. Rectification of thermal fluctuations in ideal gases. *Phys. Rev. E*, 70:051109, 2004.
- [47] Moro. Hybrid method for simulating front propagation in reaction-diffusion systems. *PHYSICAL REVIEW E*, 69(6):060101, 2004.
- [48] M. Moseler and U. Landman. Formation, stability, and breakup of nanojets. *Science*, 289(5482):1165–1169, 2000.
- [49] J.C. Nieuwoudt and B.M. Law. Theory of light scattering by a nonequilibrium binary mixture. *Phys. Rev. A*, 42(4):2003–2014, 1989.
- [50] B. Nowakowski and A. Lemarchand. Stochastic effects in a thermochemical system with newtonian heat exchange. *Phys. Rev. E*, 64(6):061108, Nov 2001.
- [51] B. Nowakowski and A. Lemarchand. Sensitivity of explosion to departure from partial equilibrium. *Physical Review E*, 68:031105, 2003.
- [52] G. Oster. Darwin’s motors. *Nature*, 417:25, 2002.
- [53] R.K. Pathria. *Statistical Mechanics*. Butterworth-Heinemann, Oxford, 1996.
- [54] G. Quentin and I. Rehberg. Direct measurement of hydrodynamic fluctuations in a binary mixture. *Phys. Rev. Lett.*, 74(9):1578–1581, Feb 1995.
- [55] Lord Rayleigh. *Scientific Papers*, volume II, pages 200–207. Cambridge, University Press, 1900.
- [56] R. Schmitz. Fluctuations in nonequilibrium fluids. *Physics Reports*, 171:1, 1988.
- [57] J. V. Sengers and J. M. Ortiz de Zrate. Thermal fluctuations in non-equilibrium thermodynamics. *Journal of Non-Equilibrium Thermodynamics*, 32(3):319–329, 2007.
- [58] D. H. Sharp. An overview of Rayleigh-Taylor instability. *Physica D Nonlinear Phenomena*, 12:3–3, July 1984.
- [59] Yoshio Sone. *Kinetic Theory and Fluid Dynamics*. Springer, 2002.
- [60] G. I. Taylor. The instability of liquid surfaces when accelerated in a direction perpendicular to their planes. *Proc. R. Soc. London Ser. A*, 201(192-196), 1950.

- [61] N. Vladimirova, A. Malagoli, and R. Mauri. Diffusion-driven phase separation of deeply quenched mixtures. *Phys. Rev. E*, 58:7691–7699, 1998.
- [62] S.A. Williams, J.B. Bell, and A.L. Garcia. Algorithm refinement for fluctuating hydrodynamics. *SIAM Multiscale Modeling and Simulation*, 6:1256–1280, 2008.
- [63] M. Wu, G. Ahlers, and D.S. Cannell. Thermally induced fluctuations below the onset of Rayleigh-Bénard convection. *Phys. Rev. Lett.*, 75(9):1743–1746, Aug 1995.